

Structure of Polymer-Stabilized Magnetic Fluids: Small-Angle Neutron Scattering and Mean-Field Lattice Modeling

Geoffrey D. Moeser,[†] William H. Green,[†] Paul E. Laibinis,[‡] Per Linse,[§] and T. Alan Hatton^{*,†}

Department of Chemical Engineering, Massachusetts Institute of Technology, Cambridge, Massachusetts 02139, Department of Chemical Engineering, Rice University, Houston, Texas 77005, and Physical Chemistry 1, Center for Chemistry and Chemical Engineering, Lund University, P.O. Box 124, S-221 00 Lund, Sweden

Received November 28, 2003. In Final Form: April 13, 2004

Small-angle neutron scattering and mean-field lattice modeling were used to characterize a class of water-based magnetic fluids tailored specifically to extract soluble organic compounds from water. The fluids consist of a suspension of ~ 7 nm magnetite (Fe_3O_4) nanoparticles coated with a bifunctional polymer layer comprised of an outer hydrophilic poly(ethylene oxide) (PEO) region for colloidal stability and an inner hydrophobic poly(propylene oxide) (PPO) region for solubilization of organic compounds. The inner region of the polymer shell is increasingly depleted of water as the fraction of PPO side chains increases. The incorporation of PPO side chains also leads to a small increase in interparticle attraction. The lattice model predicted a shell structure similar to that of a PEO–PPO–PEO triblock copolymer (Pluronic) micelle, with equivalent levels of hydration but with more PEO present in the PPO-rich regions, as the side chains grafted to the surface are less able to segregate than when in free micellar systems.

Introduction

Magnetic fluids, also known as ferrofluids, are colloidal dispersions of magnetic nanoparticles that do not settle in gravitational or moderate magnetic fields due to their small size (~ 10 nm) and do not aggregate because of their surface coatings. The nanoscale size of the particles is critical in preventing sedimentation, as Brownian motion dominates the gravitational force and the magnetic force from a typical magnet for a particle of this size.¹ The primary role of the stabilizing surfactant or polymer coating around the nanoparticles is to prevent flocculation due to the van der Waals attraction that exists between particles in a dispersion medium by providing either steric or electrostatic repulsion. Stable magnetic fluids, in which the nanoparticles remain permanently dispersed, behave as magnetically susceptible liquids and have found use in a number of commercial applications.^{2,3} Tailored magnetic fluids have been developed recently in which the stabilizing layer is modified so that, in addition to imparting colloidal stability, it provides a primary function, such as an affinity for organic compounds⁴ or proteins⁵ or the ability to reversibly bind drugs.⁶ These magnetic fluids have the potential to be used in separation processes or drug delivery applications.

We have developed water-based magnetic fluids that are specifically tailored to remove synthetic organic compounds from water.⁴ These suspensions consist of magnetite (Fe_3O_4) nanoparticles coated with a bifunctional graft copolymer composed of a poly(acrylic acid) (PAA) backbone and grafted poly(ethylene oxide) (PEO) and poly(propylene oxide) (PPO) side chains. The synthetic procedure for the graft copolymer and magnetic fluids is discussed in a previous publication.⁴ Figure 1 illustrates the synthetic procedure for the magnetic fluid and shows that the Fe_3O_4 nanoparticles are formed by precipitation of iron chlorides and coated with the graft copolymer in a single step. The PAA backbone of the graft copolymer binds to the particles just after nucleation of the Fe_3O_4 particles, preventing further growth. We hypothesize that the side chains form a bifunctional polymer shell with an outer hydrophilic PEO region that provides colloidal stability in water and an inner hydrophobic PPO region for organic solubilization. Conceptually, the resulting nanoparticles are similar to Pluronic micelles that are formed from PEO–PPO–PEO triblock copolymers⁷ and have been shown to have a high affinity for organics in their PPO-rich cores.^{8–12} We have shown that the similarities between these nanoparticles and Pluronic micelles are more than compositional, in that the solubility of many hydrophobic organics was nearly identical in the two systems when normalized for PPO content.⁴ Due to their high affinity for organics, these magnetic fluids could be

* To whom correspondence may be addressed. E-mail: tahatton@mit.edu. Tel: 617-253-4588. Fax: 617-253-8723.

[†] Massachusetts Institute of Technology.

[‡] Rice University.

[§] Lund University.

(1) Rosensweig, R. E. *Ferrohydrodynamics*, Dover Publications: Mineola, NY, 1985.

(2) Raj, K.; Moskowicz, B.; Casciari, R. *J. Magn. Magn. Mater.* **1995**, *149*, 174.

(3) Rosensweig, R. E. *Chem. Eng. Prog.* **1989**, *85*, 53.

(4) Moeser, G. D.; Roach, K. A.; Green, W. H.; Laibinis, P. E.; Hatton, T. A. *Ind. Eng. Chem. Res.* **2002**, *41*, 4739.

(5) Bucak, S.; Jones, D. J.; Laibinis, P. E.; Hatton, T. A. *Biotechnol. Prog.* **2003**, *19*, 477.

(6) Lubbe, A. S.; Bergemann, C.; Brock, J.; McClure, D. G. *J. Magn. Magn. Mater.* **1999**, *194*, 149.

(7) Alexandridis, P.; Hatton, T. A. *Colloids Surf., A* **1995**, *96*, 1.

(8) Nagarajan, R.; Barry, M.; Ruckenstein, R. *Langmuir* **1986**, *2*, 210.

(9) Hurter, P. N.; Hatton, T. A. *Langmuir* **1992**, *8*, 1291.

(10) Paterson, I. F.; Chowdhry, B. Z.; Leharne, S. A. *Langmuir* **1999**, *15*, 6187.

(11) Calvert, T. L.; Phillips, R. J.; Dungan, S. R. *AIChE J.* **1994**, *40*, 1449.

(12) Edwards, D. A.; Luthy, R. G.; Liu, Z. *Environ. Sci. Technol.* **1991**, *25*, 127.

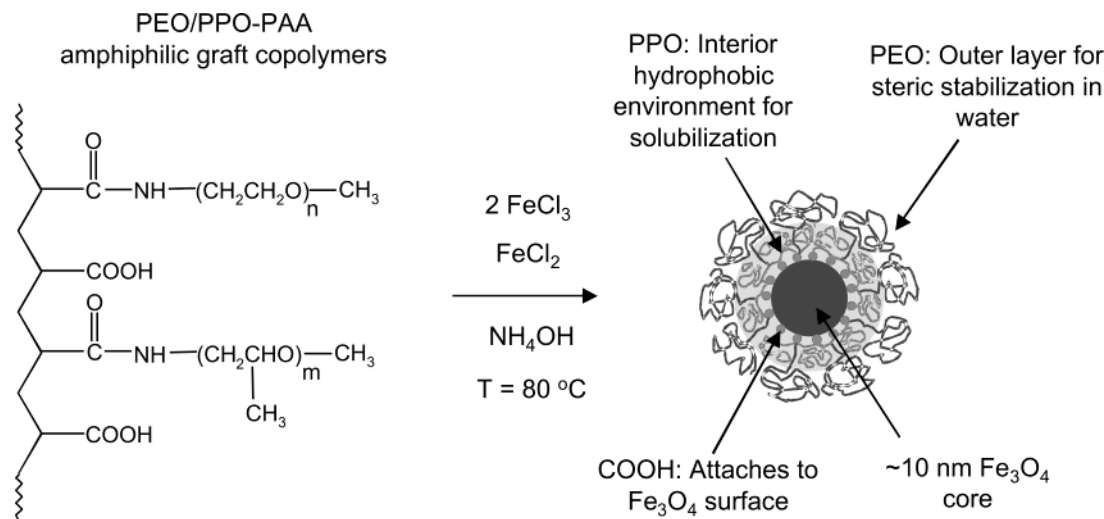


Figure 1. Aqueous magnetic fluid synthesis. The magnetic nanoparticles are produced by chemical coprecipitation of iron salts in an aqueous solution of the PEO/PPO-PAA graft copolymer. Soon after Fe_3O_4 nucleation begins, carboxylic acid groups on the PAA backbone bind to the particle surface, limiting particle growth and forming nanoparticles. The bifunctional polymer shell is formed from the hydrophilic PEO and hydrophobic PPO side chains in the graft copolymer.

used in tandem with high gradient magnetic separation^{13,14} as a novel method of organic removal from wastewater streams. The small size of the nanoparticles results in a very large exposed surface area for organic absorption that is achieved without the use of porous materials, such as activated carbon beads, that introduce a high mass transfer resistance.

The primary goal of this paper is to characterize the microstructure of the magnetic fluids with small-angle neutron scattering (SANS) and mean-field lattice modeling. Our previous characterization of the magnetic fluids⁴ yielded the dimensions of the core and shell, as well as the magnetic properties, but did not elucidate the structure within the polymer shell. In particular, we are interested in whether hydrophobic domain formation exists within the shell, such as occurs within Pluronic micelles that segregate into a core/corona structure.⁷ SANS measurements and lattice modeling provide a way of examining this internal structure.

SANS is a powerful tool for determining the structure of colloidal systems such as polymers, micelles, and nanoparticle dispersions.¹⁵ In this technique, the size and composition of a structure, as well as interactions, are deduced from the neutron scattering pattern of a sample. A key feature of SANS is that it allows different regions of a structure to be probed independently through selective deuteration of the sample. The large difference in neutron scattering from hydrogen and deuterium results in significant changes in the scattering pattern when deuterated materials are used in place of hydrogenated materials. This technique, known as contrast matching, relies on the fact that deuteration of water does not significantly alter its solvation of many polymers.¹⁶ In this work, we prepare magnetic fluids in H_2O -rich and D_2O -rich solvents to isolate scattering from the Fe_3O_4 core and polymer shell, respectively. Scattering from the polymer shell can be used to deduce the water penetration into the shell, giving information about the presence of

hydrophobic domains. Previous work on SANS analysis of magnetic fluids has demonstrated the feasibility of using this technique to probe the size, structure, and aggregation behavior of the particles.^{17–19} Likewise, SANS has been shown to be an excellent tool in identifying hydrophobic domains in micellar systems composed of PEO-PPO-PEO triblock copolymers.^{16,20,21}

Mean-field lattice theory provides a very useful framework to model the structure of polymer layers near surfaces and interfaces as well as across interfaces. This theory was originally developed by Scheutjens and Fleer,²² and it has later been extended in numerous directions. The inclusion of the concept of internal degrees of freedoms²³ into the lattice theory^{24,25} has triggered an extensive modeling of the solution behavior of mixtures of PEO and PPO,²⁶ the micellization of PEO-PPO-PEO triblock copolymers,^{27–30} the structure of PEO-PPO-PEO triblock copolymers adsorbed at surfaces,^{25,31} and terminally grafted PEO chains at interfaces.^{24,32} An application of this theory to describe the polymer shell around the magnetite nanoparticles represents a combination of several of these systems, suggesting that lattice modeling should be able to provide information about hydrophobic domain formation in the polymer shell. As we will see, such modeling yields (i) the volume fraction profile of

(17) Shen, L. F.; Stachowiak, A.; Fateen, S. E. K.; Laibinis, P. E.; Hatton, T. A. *Langmuir* **2001**, *17*, 288.

(18) Cebula, D. J.; Charles, S. W.; Popplewell, J. *Colloid Polym. Sci.* **1981**, *259*, 395.

(19) Hayter, J. B. *J. Chem. Soc. Faraday Trans.* **1991**, *87*, 403.

(20) Goldmints, I.; Yu, G. E.; Booth, C.; Smith, K. A.; Hatton, T. A. *Langmuir* **1999**, *15*, 1651.

(21) Liu, Y. C.; Chen, S. H.; Huang, J. S. *Macromolecules* **1998**, *31*, 2236.

(22) Scheutjens, J.; Fleer, G. J. *J. Phys. Chem.* **1979**, *83*, 1619.

(23) Karlstrom, G. *J. Phys. Chem.* **1985**, *89*, 4962.

(24) Bjorling, M.; Linse, P.; Karlstrom, G. *J. Phys. Chem.* **1990**, *94*, 471.

(25) Linse, P.; Bjorling, M. *Macromolecules* **1991**, *24*, 6700.

(26) Malmsten, M.; Linse, P.; Zhang, K. W. *Macromolecules* **1993**, *26*, 2905.

(27) Linse, P. *J. Phys. Chem.* **1993**, *97*, 13896.

(28) Linse, P. *Macromolecules* **1993**, *26*, 4437.

(29) Hurter, P. N.; Scheutjens, J.; Hatton, T. A. *Macromolecules* **1993**, *26*, 5592.

(30) Hurter, P. N.; Scheutjens, J.; Hatton, T. A. *Macromolecules* **1993**, *26*, 5030.

(31) Linse, P.; Hatton, T. A. *Langmuir* **1997**, *13*, 4066.

(32) Baskir, J. N.; Hatton, T. A.; Suter, U. W. *Macromolecules* **1987**, *20*, 1300.

(13) Gerber, R.; Birss, R. R. *High Gradient Magnetic Separation*; Research Studies Press: London, U.K., 1983.

(14) Moesser, G. D.; Roach, K. A.; Green, W. H.; Laibinis, P. E.; Hatton, T. A. *AIChE J.* **2003**.

(15) Feigin, L. A.; Svergun, D. I. *Structural Analysis by Small-Angle X-ray and Neutron Scattering*; Plenum Press: New York, 1987.

(16) Goldmints, I.; vonGottberg, F. K.; Smith, K. A.; Hatton, T. A. *Langmuir* **1997**, *13*, 3659.

grafted polymer chains and water in the shell, which will be compared to the water penetration profile extracted from SANS data, and (ii) the PEO–PPO segregation inside the polymer shell, a feature not observable with neutron scattering from nondeuterated polymers because of the similarities of the nuclear scattering length densities of EO and PO monomers.

Experimental Section

Materials. Poly(acrylic acid) (50 wt % in water, $M_w = 5000$), iron(III) chloride hexahydrate (97%), iron(II) chloride tetrahydrate (99%), ammonium hydroxide (28 wt % in water), hydrochloric acid (37 wt % in water), and Tiron (4,5-dihydroxy-1,3-benzene-disulfonic acid, disodium salt monohydrate) were obtained from Sigma-Aldrich (Milwaukee, WI). Deuterium oxide (D_2O) was supplied by Cambridge Isotope Laboratories (Andover, MA). Jeffamine XTJ-234 ($CH_3-O-PEO/PPO-NH_2$, EO:PO = 6.1:1, $M_w = 3000$) and Jeffamine XTJ-507 ($CH_3-O-PEO/PPO-NH_2$, EO:PO = 1:6.5, $M_w = 2000$) were obtained as gifts from Huntsman Corporation (Houston, TX). In this work, we consider the random copolymer XTJ-234 to be equivalent to pure PEO and XTJ-507 to be equivalent to pure PPO, and we refer to these polymers as PEO– NH_2 and PPO– NH_2 , respectively.

Preparation of Magnetic Fluids. A detailed description of the synthetic procedure for the magnetic fluids is given in a previous publication.⁴ In summary, the graft copolymer that forms the polymer shell was synthesized by reacting PAA with PEO– NH_2 and PPO– NH_2 via an amidation reaction. The stoichiometry of this reaction was selected so that 16% of the carboxylic acid groups on the PAA backbone (in total) were substituted with PEO– NH_2 and PPO– NH_2 side chains. By varying the PEO/PPO composition in the reaction, we produced 16/0, 12/4, and 8/8 polymers, where the nomenclature x/y refers to a magnetic fluid produced with a graft copolymer in which $x\%$ of the carboxylic acid groups in the PAA backbone were reacted with PEO chains and $y\%$ with PPO chains. The 16/0, 12/4, and 8/8 polymer-coated nanoparticles were then produced by coprecipitation of iron(II) and iron(III) chloride to form magnetite in the presence of the corresponding graft copolymer, as shown in Figure 1. Nanoparticles are formed because the polymer binds to the magnetite surface just after particle nucleation, thereby limiting particle growth.

To prepare the suspensions for the SANS experiments, the magnetic fluids were washed by diluting them to 0.5 wt % Fe_3O_4 with distilled water and then concentrating them to 2.5 wt % in a 100 000 molecular weight cutoff centrifugal filter (Millipore). The polymer-coated nanoparticles were retained by the filter while unattached polymer and ionic species were lost in the filtrate. This process of dilution and concentration in the filter was repeated four times to fully remove free polymer and ions, which was confirmed by evaporating the filtrate until there was no residual mass. All three magnetic fluids were diluted to 0.5 wt % Fe_3O_4 after washing and then placed on a 0.5 T permanent magnet for 1 h to remove aggregates or uncoated particles. The exact magnetite concentration in the magnetic fluids was determined by iron titration.³³ The final suspensions for SANS were produced by evaporating five 4 mL portions of each magnetic fluid under a flow of nitrogen gas. Each magnetic fluid was then resuspended in 4 mL of five different H_2O/D_2O mixtures of varying composition by mild sonication in a water bath for 5 min. Specifically, each magnetic fluid was resuspended in mixtures that contained 100, 75, 50, 25, and 0 vol % H_2O . The 8/8 magnetic fluid was also prepared in a solvent mixture with 82 vol % H_2O .

Electron Microscopy Measurements. Transmission electron microscopy (TEM) experiments were performed on a JEOL 2010 (200 kV) instrument. Samples were prepared by evaporating dilute suspensions on a carbon-coated film. The median size and polydispersity of the magnetite particles was determined by measuring 150 particles.

SANS Measurements. Small-angle neutron scattering experiments were conducted on the NG3 30 m SANS instrument at the National Institute of Standards and Technology (NIST) in Gaithersburg, MD. An unpolarized neutron beam with an

average wavelength (λ) of 6 Å and a wavelength spread ($\Delta\lambda/\lambda$) of 0.11 was used in all scattering experiments. Samples were loaded in quartz cells with a path length of 1 mm. Scattering experiments were conducted on each sample at two sample-to-detector distances (1.33 and 7.00 m) with a lateral detector offset of 0.25 m, yielding a continuous q range of $0.005 \leq q \leq 0.4 \text{ \AA}^{-1}$ for each sample. The scattering intensity on the detector was circularly averaged for each scattering angle because the scattering was observed to be isotropic. Scattering from the solvent and empty cell was subtracted by measuring the scattering from pure solvent in an identical cell. The scattering was placed on an absolute scale with the use of standards and software supplied by NIST.

Scattering Theory

General Scattering Equations. In small-angle neutron scattering experiments on magnetic fluids, neutrons interact with and are scattered by both atomic nuclei and the magnetic dipoles of the atoms. In the absence of an external magnetic field, the magnetic dipoles are randomly oriented in the suspension, and the nuclear and magnetic scattering contributions are additive, with the total coherent scattering intensity $I(q)$ given by^{17,18}

$$I(q) = N_p (|F_N(q)|^2 + 2/3|F_M(q)|^2) S(q) \quad (1)$$

where N_p is the number density of particles in the suspension, F_N is the nuclear particle form factor, F_M is the magnetic particle form factor, and $S(q)$ is the interparticle structure factor. The F_N and F_M terms are a result of coherent scattering from the particle nuclei and magnetic dipoles, respectively, and are functions of particle size and shape, while $S(q)$ depends on the pair correlation function between particles (and therefore the interparticle interaction potential). The $2/3$ factor that multiplies the magnetic form factor is a result of averaging over all orientations of the magnetic dipole in the absence of a magnetic field.¹⁸ The scattering vector q is related to the scattering angle θ by

$$q = \frac{4\pi}{\lambda} \sin\left(\frac{\theta}{2}\right) \quad (2)$$

For a polydisperse system, the total scattering intensity is given by integrating over all particles in the suspension according to

$$I(q) = \bar{N}_p \int_0^\infty (|F_N(q)|^2 + 2/3|F_M(q)|^2) p(R_c) dR_c S(q) \quad (3)$$

The normalized probability density $p(R_c)$ will in the following be assumed to take the log-normal distribution form⁴

$$p(R_c) = \frac{1}{(2\pi)^{1/2} \sigma_c R_c} \exp\left[-\frac{1}{2\sigma_c^2} (\ln(R_c/R_{c,med}))^2\right] \quad (4)$$

with a median core radius, $R_{c,med}$, and a core polydispersity, σ_c . The average particle number density is given by

$$\bar{N}_p = \frac{\phi_{mag}}{4/3\pi \int_0^\infty R_c^3 p(R_c) dR_c} \quad (5)$$

where ϕ_{mag} is the total volume fraction of magnetite in the suspension. The structure factor $S(q)$ is assumed to be unaffected by polydispersity.¹⁷

Form Factor Models. The nuclear and magnetic form factors of a particle originate from the scattering from all atoms in the particle and hence allow $I(q)$ measurements

Table 1. Scattering Length Densities (SLD) for Materials in the Magnetic Fluids

material	SLD (10^{-6} \AA^{-2})	
	nuclear	magnetic
Fe ₃ O ₄	6.96 ^a	1.36
polymer	0.76	
H ₂ O	-0.56 ^a	
D ₂ O	6.36 ^a	

^a Nuclear SLD value from ref 17.

to be used to infer the structure within a particle as well as the size and shape of the particle. The scattering of a material is defined by its scattering length density (SLD), which is a material property related to the stoichiometry, density, nuclear spin state, and magnetization of the material. The nuclear SLDs (ρ_N) of the compounds in our magnetic fluids are summarized in Table 1. The graft copolymer is treated as a single component with average nuclear SLD of $0.76 \times 10^{-6} \text{ \AA}^{-2}$ because the nuclear SLDs of PEO ($0.57 \times 10^{-6} \text{ \AA}^{-2}$) and PPO ($0.35 \times 10^{-6} \text{ \AA}^{-2}$) are so similar as to make distinguishing between them by SANS extremely difficult,¹⁶ while PAA ($2.4 \times 10^{-6} \text{ \AA}^{-2}$) makes up less than 10 vol % of the graft copolymer. Similarly, solvent mixtures of H₂O and D₂O have a composition-weighted average nuclear SLD.

The magnetic SLD (ρ_M) of a material is given by^{19,34}

$$\rho_M = b_M M_s \quad (6)$$

where b_M is the magnetic scattering length per Bohr magneton ($= 2.318 \times 10^{14} \text{ T}^{-1} \text{ m}^{-2}$) and M_s is the saturation magnetization of the bulk material (in tesla). With $M_s = 0.60 \text{ T}$ (87 emu/g) for magnetite, the magnetic SLD for magnetite is $1.36 \times 10^{-6} \text{ \AA}^{-2}$, which is consistent with other reports.³⁴ The polymer shell and the H₂O and D₂O solvents have negligible magnetization, and hence ρ_M is zero for these components.

The form factor for a particle with spherical symmetry is³⁵

$$F(q) = 4\pi \int_0^\infty (\rho(r) - \rho_s) \frac{\sin(qr)}{qr} r^2 dr \quad (7)$$

where $\rho(r)$ is the scattering length density of the atoms at distance r from the particle center and ρ_s is the scattering length density of the solvent (outside the particle). Equation 7 holds for both the nuclear (F_N) and the magnetic (F_M) form factors, with nuclear and magnetic SLD profiles $\rho_N(r)$ and $\rho_M(r)$, respectively.

We consider the two different models for the particle structure shown in Figure 2. In both cases, the core of radius R_c consists of pure magnetite and is surrounded by a hydrated polymer shell of length L_1 . In case a, we assume a linear solvent penetration profile, with the solvent volume fraction varying from ϕ_{s1} at the magnetite surface to unity at the outer edge of the shell. When the radial variation in the SLD, $\rho_N(r)$, within the shell is accounted for, the nuclear form factor (eq 7) becomes

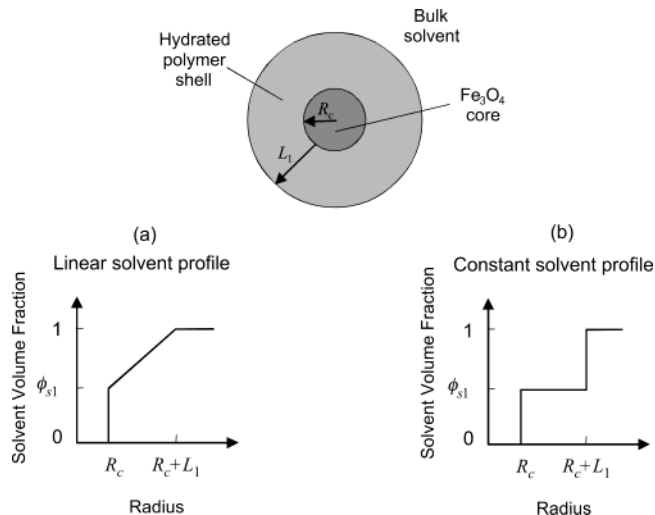


Figure 2. Solvent penetration models for the magnetic nanoparticle form factor: (a) linear and (b) constant solvent volume fraction profile in the polymer shell.

$$F_N(q) = \frac{4\pi}{q} \left\{ R_c^2 \left(\rho_{Nc} - \frac{\rho_{N1}(R_c + L_1) - \rho_{Ns}R_c}{L_1} \right) j_1(qR_c) + \left(\frac{\rho_{Ns} - \rho_{N1}}{L_1} \right) \left(\frac{2(R_c + L_1)}{q^2} \sin(q(R_c + L_1)) - \frac{2R_c}{q^2} \sin(qR_c) \right) + \left(\frac{\rho_{Ns} - \rho_{N1}}{L_1} \right) \left(-\frac{q^2(R_c + L_1)^2 - 2}{q^3} \cos(q(R_c + L_1)) + \frac{q^2 R_c^2 - 2}{q^3} \cos(qR_c) \right) + (R_c + L_1)^2 \times \left(\frac{\rho_{N1}(R_c + L_1) - \rho_{Ns}R_c}{L_1} - \rho_{Ns} \right) j_1(q(R_c + L_1)) \right\} \quad (8)$$

where $j_1(x) = (\sin x - x \cos x)/x^2$ is a first-order spherical Bessel function, and ρ_{N1} , ρ_{Nc} , and ρ_{Ns} are the nuclear SLDs in the polymer shell at the magnetite surface, of the magnetite core, and of the solvent, respectively.

In case b, the solvent penetration is assumed to be homogeneous, with a constant solvent volume fraction of ϕ_{s1} in the shell. In this case, the nuclear SLD of the polymer shell (ρ_{N1}) is given by a weighted average of the solvent and polymer volume fractions in the shell

$$\rho_{N1} = \phi_{s1} \rho_{Ns} + (1 - \phi_{s1}) \rho_{Np} \quad (9)$$

where ρ_{Np} is the nuclear SLD of the polymer. The nuclear form factor reduces to the well-known form factor for core-shell particles^{16,17}

$$F_N(q) = \frac{4\pi}{q} [R_c^2 (\rho_{Nc} - \rho_{N1}) j_1(qR_c) + (R_c + L_1)^2 \times (\rho_{N1} - \rho_{Ns}) j_1(q(R_c + L_1))] \quad (10)$$

The polydispersity of the Fe₃O₄ particles also affects the polymer shell thickness due to curvature effects. For a constant polymer grafting density, the shell thickness increases with increasing core radius because of decreasing curvature.^{36,37} The scaling behavior of the shell thickness from these models is relatively complex but in the size range of our nanoparticles can be approximated as⁴²

(34) Lembke, U.; Hoell, A.; Kranold, R.; Muller, R.; Schuppel, W.; Goerigk, G.; Gilles, R.; Wiedenmann, A. *J. Appl. Phys.* **1999**, *85*, 2279.

(35) Eastoe, J.; Hetherington, K. J.; Sharpe, D.; Dong, J. F.; Heenan, R. K.; Steytler, D. *Langmuir* **1996**, *12*, 3876.

(36) Farinha, J. P. S.; d'Oliveira, J. M. R.; Martinho, J. M. G.; Xu, R. L.; Winnik, M. A. *Langmuir* **1998**, *14*, 2291.

(37) Lin, E. K.; Gast, A. P. *Macromolecules* **1996**, *29*, 390.

$$L_1 = L_{1,\text{med}} \left(\frac{R_c}{R_{c,\text{med}}} \right)^{0.24} \quad (11)$$

where $L_{1,\text{med}}$ is the shell thickness of a particle with the median core radius $R_{c,\text{med}}$.

For the magnetic scattering, the form factor for spherical particles of constant SLD is used, with the one caveat that we account for a nonmagnetic shell of thickness $\delta = 8.3 \text{ \AA}$ at the exterior of the magnetite core,¹⁷ which is usually ascribed to the disruption of the electronic structure of the atoms at the surface.¹ The magnetic form factor is, therefore, given by

$$F_M(q) = \frac{4\pi}{q} (R_c - \delta)^2 \rho_{\text{Mc}} j_1(q(R_c - \delta)) \quad (12)$$

where ρ_{Mc} is the magnetic SLD of the magnetite core. As a result of the low magnetic SLD of magnetite compared to the nuclear SLD, the magnetic scattering is 1–2 orders of magnitude lower than the nuclear scattering in all solvents used in this study; we include it here for the sake of completeness.

Structure Factor Model. Dynamic light scattering (DLS) studies have indicated that our nanoparticles have a tendency to aggregate.⁴ These attractive interactions were accounted for using the Ornstein–Zernike structure factor³⁸

$$S(q) = 1 + \frac{S_0}{1 + (q\zeta)^2} \quad (13)$$

where S_0 is related to the osmotic compressibility of the suspension (increases with increasing attractive force) and ζ is the correlation length of the interaction. This structure factor has been applied successfully to systems of PEO-containing microemulsions that tend to aggregate.³⁹

SANS Fitting Approach. All magnetic fluids used in this study were prepared in five H₂O/D₂O mixtures with compositions ranging from pure H₂O to pure D₂O. Previous studies have shown that the level of deuteration in the aqueous solvent does not significantly affect the structure of Pluronic micelles, which are composed of PEO and PPO chains similar to those used in our graft copolymers.¹⁶ The mixtures of H₂O and D₂O are used to vary the solvent SLD without changing the hydration of the polymer shell or the structure of the particles. This method of contrast variation allowed isolation of different parts of the nanoparticles by matching the solvent SLD to either the graft copolymer (isolating scattering from the magnetite core) or the magnetite core (isolating scattering from the solvated polymer shell). The data fitting approach was to use a single contrast-matched solvent to extract the core parameters and a global fit over a range of solvent conditions to determine the shell and interparticle parameters. A χ^2 fit was used in all data fitting procedures, as the NIST software provided estimates of the standard deviation of the measured intensity at each point. Generally, $\chi^2/N < 1$ is required for a good fit in which the model is within the measurement error for all points,⁴⁰ although this is not always possible for global fits of different solvent

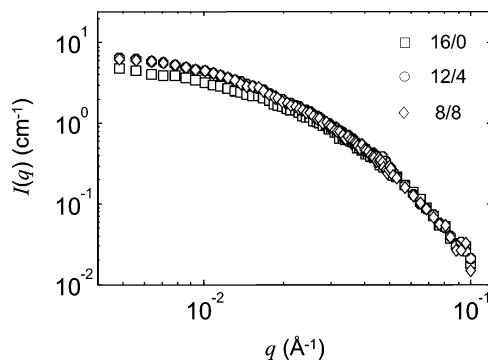


Figure 3. Neutron scattering data for the magnetic fluid containing 16/0, 12/4, and 8/8 particles in 75% H₂O/25% D₂O. At $q \geq 0.03 \text{ \AA}^{-1}$ the scattering is very similar, suggesting a similar Fe₃O₄ core size for all particles.

SLDs.⁴¹ Our data fitting was limited to points with $q \leq 0.1 \text{ \AA}^{-1}$ as the scattering above this range was primarily incoherent background.

SANS Results

Determination of Core Parameters. Transmission electron microscopy (TEM) measurements demonstrated that the magnetite core is approximately spherical and polydisperse,⁴ with median core diameter of 7.3 nm ($R_{c,\text{med}} = 36 \text{ \AA}$) and a polydispersity, σ_c , of 0.30. No significant differences in these parameters for the 16/0, 12/4, and 8/8 magnetic fluids were observed, which is consistent with results from magnetization measurements.⁴ The current SANS results also indicate that the core size is independent of polymer coating composition. Figure 3 shows scattering data for the three types of magnetic fluids in a solvent composed of 75% H₂O and 25% D₂O. For this mixture, $\rho_{\text{Ns}} = 1.17 \times 10^{-6} \text{ \AA}^{-2}$, which is close to the SLD, ρ_{Np} , of the graft copolymers ($0.76 \times 10^{-6} \text{ \AA}^{-2}$), so that scattering becomes dependent only on the magnetite core, as shown by eq 10. For $q > 0.03 \text{ \AA}^{-1}$, the scattering profiles of the 16/0, 12/4, and 8/8 particles coincide, suggesting that the magnetite cores are essentially identical. The scattering at lower q , where larger scale structures dominate, increases somewhat from 16/0 to 8/8, attributed to differences in interparticle interactions as reflected in the structure factor $S(q)$, which will be discussed further in the next section. The error bars, reflecting any alignment errors, variation in the neutron beam source intensity, and other sources of random noise such as detector electronics, are all generally smaller than the symbols used to represent the measured spectral data.

The median size of the Fe₃O₄ core was determined from the scattering profile shown in Figure 4 for an 8/8 magnetic fluid in a solvent composed of 82% H₂O and 18% D₂O. This solvent has a nuclear SLD of $0.69 \times 10^{-6} \text{ \AA}^{-2}$, close to that of the polymer itself, such that only the cores scattered neutrons, and the nuclear form factor is simply that for homogeneous spheres

$$F_N(q) = \frac{4\pi}{q} R_c^2 (\rho_{\text{Nc}} - \rho_{\text{Ns}}) j_1(qR_c) \quad (14)$$

The scattering data confirm TEM and magnetization measurements of particle size distributions that indicate the magnetic fluid nanoparticles are polydisperse, in that oscillations in the scattering profiles that would be

(38) Kotlarchyk, M.; Chen, S. H.; Huang, J. S. *Phys. Rev. A* **1983**, *28*, 508.

(39) Schubel, D.; Bedford, O. D.; Ilgenfritz, G.; Eastoe, J.; Heenan, R. K. *Phys. Chem. Chem. Phys.* **1999**, *1*, 2521.

(40) Press, W. H.; Teukolsky, S. A.; Flannery, B. P.; Vetterling, W. T. *Numerical Recipes: The Art of Scientific Computing*; Cambridge University Press: Cambridge, 1989.

(41) Won, Y. Y.; Davis, H. T.; Bates, F. S.; Agamalian, M.; Wignall, G. D. *J. Phys. Chem. B* **2000**, *104*, 7134.

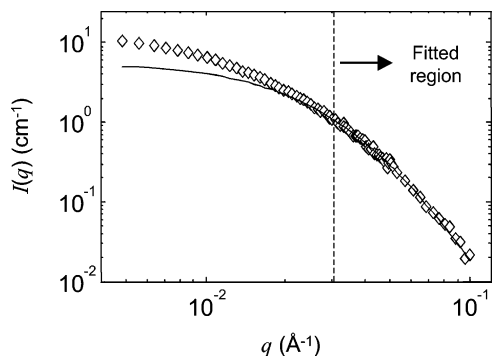


Figure 4. Neutron scattering data for the magnetic fluid containing 8/8 particles in 82% H₂O/18% D₂O. This solvent matches the scattering length density of the graft copolymer. The solid line represents the best fit of the data in the range $0.03 < q < 0.1 \text{ \AA}^{-1}$ by varying $R_{c,med}$, σ_c , and ϕ_{mag} . Error bars are smaller than the symbols in all cases.

observed for monodisperse spheres are smeared by the broad distribution of core sizes.¹⁷

The parameters $R_{c,med}$, σ_c , and ϕ_{mag} were extracted by fitting the scattering model to the scattering data over the range $0.03 < q < 0.1 \text{ \AA}^{-1}$; as shown in Figure 4, the fit is excellent (in the fitted region) with $\chi^2/N = 0.88$. The scattering is underpredicted at low q (outside the fitted range) due to interparticle interactions, as will be discussed in more detail in the next section. The optimal values of the fitted parameters were $R_{c,med} = 24 \text{ \AA}$, $\sigma_c = 0.49$, and $\phi_{mag} = 9.3 \times 10^{-4}$. ϕ_{mag} is effectively a scale factor for the scattering and was acceptably close to the magnetite volume fraction in the magnetic fluid as measured by iron titration (1.09×10^{-3}). The median core radius from SANS is lower than the value of 36 \AA determined from TEM images of the same sample, while the core polydispersity is higher than the value of 0.30 from TEM.

The source of this core size discrepancy is uncertain, but a likely explanation is that the differences are due to irregularities in the shapes of the magnetic particles. The TEM images of the nanoparticles in Figure 5 show that while some particles are spherical, others are more ellipsoidal in nature or have angular surfaces. In measurements of the diameters of ellipsoidal particles from TEM images, an average of the two principle radii was used. Shen et al.¹⁷ have shown when such ellipsoidal particles are modeled as equivalent spheres in SANS analyses, the extracted sizes are lower than those obtained using this arithmetic average of the two principle radii, as has been observed here. A fit of the data in Figure 4 with a form factor for polydisperse ellipsoids (with radii a , a , and b) resulted in the median primary radius, a_{med} , increasing to 33.2 \AA with an axial ratio b/a of 0.50 , but excessive polydispersity was still observed ($\sigma_c = 0.480$) and the quality of the fit did not improve.

Global Fit of Shell Parameters. The hydration profile of the polymer shell around the nanoparticles and the parameters that define the interparticle interactions were determined by a global fit of the SANS data for each type of particle in five H₂O/D₂O mixtures with a varying level of deuteration. The effective size of the Fe₃O₄ core and the magnetite volume fraction determined above were held constant in all the fits. Thus, the globally fitted parameters were the shell thickness of a median particle ($L_{1,med}$), the shell solvent volume fraction parameter (ϕ_{s1}), and the two parameters that characterized interparticle interactions (S_0 and ζ). Global fits were performed for each type of particle assuming linear (Figure 2a) and constant (Figure 2b) solvent profiles. In the former case, ϕ_{s1} is the solvent

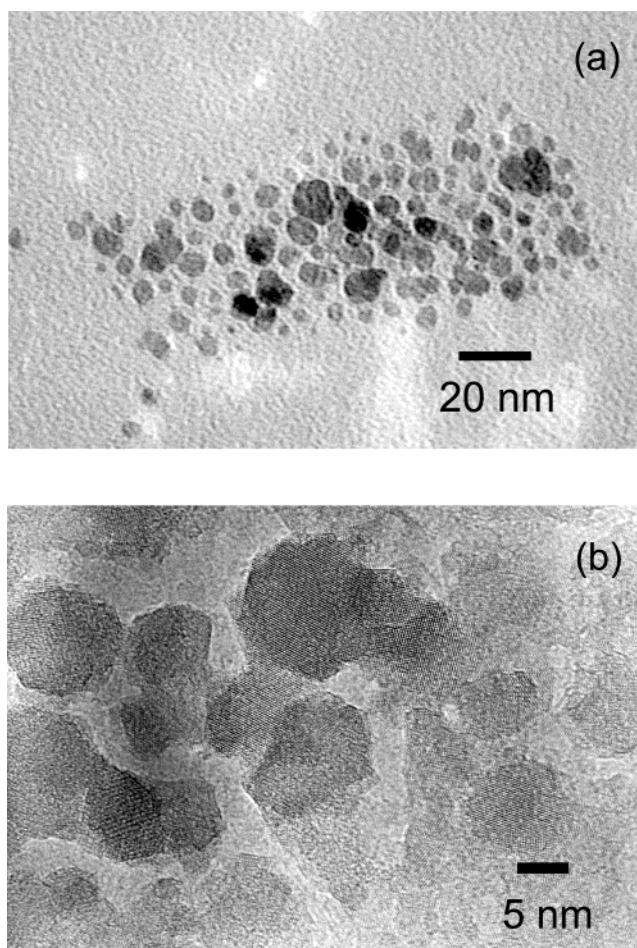


Figure 5. (a) TEM image of the 16/0 particles. (b) High-resolution TEM image of the 16/0 particles, showing the atomic planes in the nanoparticles and the angular surfaces.

volume fraction at the Fe₃O₄ interface, while in the latter case it is the solvent volume fraction throughout the polymer shell. The simultaneous fitting of five data series using four fitting parameters ensured a higher level of confidence in the parameters. The fitted parameters, $L_{1,med}$, ϕ_{s1} , S_0 , and ζ , were found to be relatively independent of the core shape and size, changing by less than 2% when the particles were modeled as core-shell ellipsoids rather than as spheres.

The scattering intensities for the three types of particles in the five solvents ranging from H₂O to D₂O are shown in Figure 6. For clarity, the scattering curves in the various solvents are offset by factors of 10 going from H₂O to D₂O. The actual order of the scattering intensities as $q \rightarrow 0$ in the various solvents is 100% H₂O > 0% H₂O > 75% H₂O > 25% H₂O > 50% H₂O. This itself is evidence of the scattering from the polymer shell, as bare magnetite particles would show decreasing scattering with increasing solvent deuteration. The shape of the scattering data also shows evidence of the polymer shell. The H₂O-rich solvents, where the scattering is primarily from the Fe₃O₄ core, show a monotonic decay consistent with polydisperse spheres. The scattering in the D₂O-rich solvents, which is primarily due to the polymer shell, shows some evidence of a shoulder, although very distinguishable features are smeared by the high polydispersity.

The best global fits of the scattering data for the three cases assuming linear solvent volume fraction profiles are shown as the solid lines in Figure 6. The optimal values of the fitted parameters and the total χ^2 error are summarized in Table 2 for these three magnetic fluids.

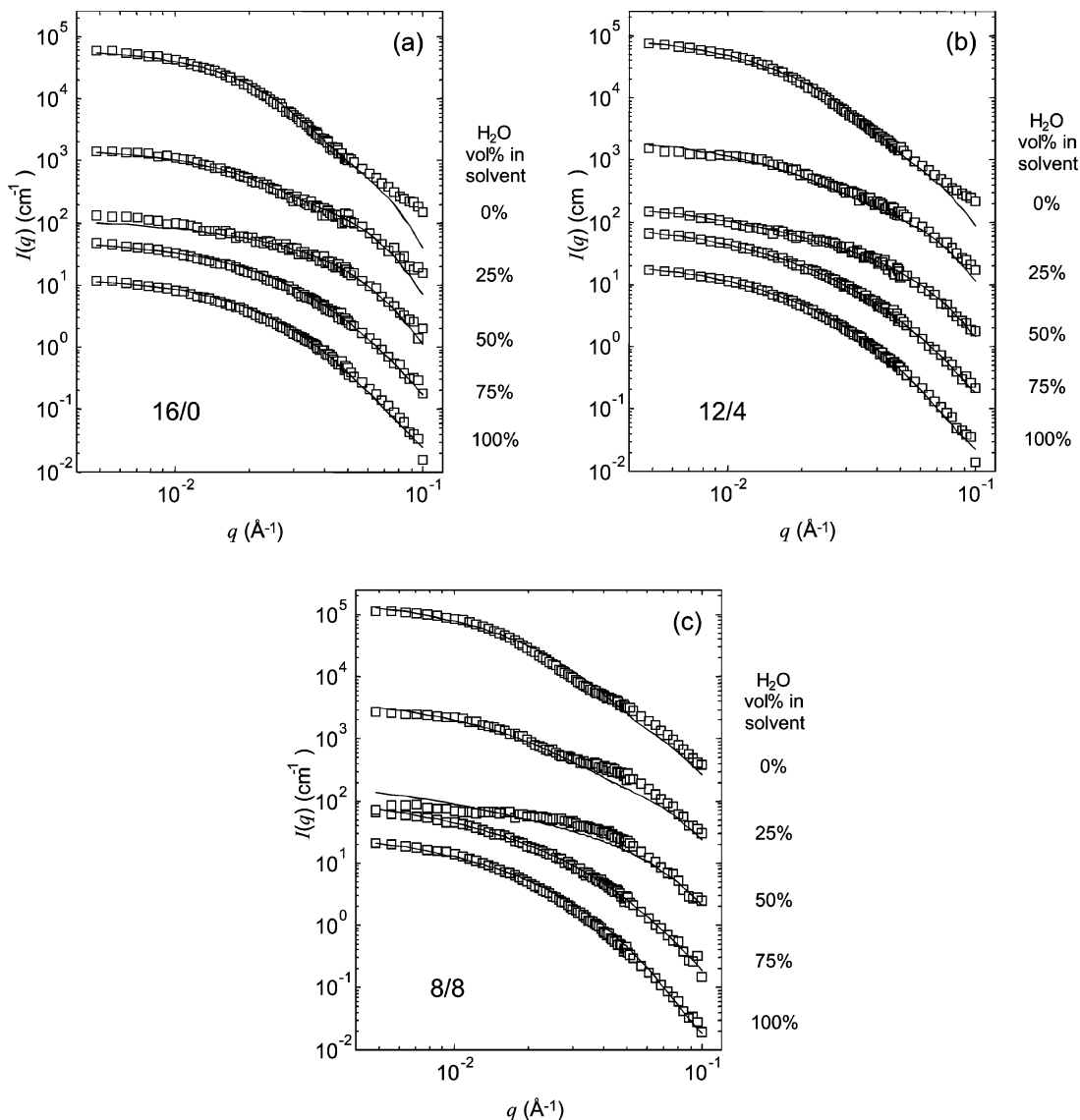


Figure 6. Neutron scattering data for the magnetic fluid containing (a) 16/0, (b) 12/4, and (c) 8/8 particles in five aqueous solvents with a varying level of deuteration. The curves are offset for clarity by factors of 100% H₂O ($\times 1$), 75% H₂O ($\times 10$), 50% H₂O ($\times 100$), 25% H₂O ($\times 10^3$), 0% H₂O ($\times 10^4$). The solid lines represent a global fit with the linear solvent model (Figure 2a) to the five data series over the whole q range by varying $L_{1,\text{med}}$, ϕ_{s1} , S_0 , and ζ . The predicted scattering was calculated with the form factor in eq 8. The error bars on the scattering data are smaller than the symbols in all cases.

Table 2. Results of Global Fit Assuming a Linear Solvent Volume Fraction in Shell

property	values inferred from SANS data			values measured with other technique
	16/0	12/4	8/8	
χ^2/N	11.6	10.4	57.8	
$R_{c,\text{med}}$ (Å)	24.1	24.1	24.1	36 ^a
σ_c	0.490	0.490	0.490	0.30 ^a –0.35 ^b
ϕ_{mag}	9.29×10^{-4}	9.29×10^{-4}	9.29×10^{-4}	1.09×10^{-3} ^c
$L_{1,\text{med}}$ (Å)	61.5	50.8	41.0	94 ^d
ϕ_{s1}	0.632	0.521	0.185	
S_0	0.210	1.13	1.47	
ζ (Å)	130	129	140	
m_p/m_m	0.482	0.442	0.523	0.80 ^e

^a Transmission electron microscopy. ^b Magnetization analysis. ^c Iron titration. ^d Dynamic light scattering. ^e Thermogravimetric analysis.⁴²

The constrained effective core parameters are also shown in italics, along with values determined by other experimental methods.^{4,42} The fit is generally good for 16/0 and 12/4 particles, with χ^2/N values of 11.6 and 10.4, respectively. The global fit of the 8/8 data is somewhat worse,

with a χ^2/N value of 57.8. These χ^2/N values imply that the predicted scattering was outside the measurement uncertainty for some points, although the fits are generally acceptable and capture the important features of the data. The fit for the 16/0 particles is weakest at high q in the D₂O-rich solvents, which is probably caused by our use of a core–shell model for the particle structure, resulting in a predicted q^{-4} scattering dependence at high q . Blob structure in the polymer shell (internal structure not considered in our development) has been reported to cause the scattering to decay at approximately q^{-2} at q greater than $0.06\text{--}0.10 \text{ \AA}^{-1}$,^{43–45} which is the region in which our predicted scattering begins to diverge in the D₂O-rich samples. As we limited our fit to $q < 0.1 \text{ \AA}^{-1}$, neglecting blob scattering should not lead to significant errors. The

(42) Moeser, G. D. *Colloidal Magnetic Fluids as Extractants for Chemical Processing Applications*; Massachusetts Institute of Technology: Cambridge, 2003.

(43) Pedersen, J. S.; Svaneborg, C. *Curr. Opin. Colloid Interface Sci.* **2002**, *7*, 158.

(44) Poppe, A.; Willner, L.; Allgaier, J.; Stellbrink, J.; Richter, D. *Macromolecules* **1997**, *30*, 7462.

(45) Forster, S.; Burger, C. *Macromolecules* **1998**, *31*, 879.

Table 3. Results of Global Fit Assuming a Constant Solvent Volume Fraction in Shell

property	values inferred from SANS data			values measd with other technique
	16/0	12/4	8/8	
χ^2/N	10.6	6.40	43.2	
$R_{c,med}$ (Å)	24.1	24.1	24.1	36 ^a
σ_c	0.490	0.490	0.490	0.30 ^a –0.35 ^b
ϕ_{mag}	9.29×10^{-4}	9.29×10^{-4}	9.29×10^{-4}	1.09×10^{-3} ^c
$L_{1,med}$ (Å)	45.3	39.8	33.3	94 ^d
ϕ_{s1}	0.768	0.720	0.537	-
S_0	0.237	1.08	1.35	-
ζ (Å)	130	124	133	-
m_p/m_m	0.477	0.452	0.543	0.80 ^e

^a Transmission electron microscopy. ^b Magnetization analysis.⁴
^c Iron titration. ^d Dynamic light scattering.⁴ ^e Thermogravimetric analysis.⁴²

main source of error from the 8/8 particles appears to be from the scattering in D₂O-rich solvents at intermediate q , where the shoulder due to shell scattering is not captured perfectly.

The results of repeating the global fit of the neutron scattering data with the constant solvent penetration model (Figure 2b) are summarized in Table 3. A comparison of χ^2/N for the linear (Table 2) and constant solvent profiles shows that changing the solvent penetration model did not have a strong effect on the quality of fit.

In Tables 2 and 3, a clear trend is seen in the fitted parameters $L_{1,med}$ and ϕ_{s1} that characterize the solvation of the polymer shell, in that the shell contracts and becomes less solvated with increasing PPO fraction. The presence of the PPO reduces the hydration of the PEO chains, decreasing the H₂O/EO molar ratio from 9.3 for the 16/0 particles to 5.6 for the 8/8 particles. These values compare with those for Pluronic micelles, which typically have an H₂O/EO ratio of 3–9 depending on composition and temperature.²¹

The shell thickness from SANS (~40–60 Å) was significantly smaller than that inferred from dynamic light scattering measurements (~94 Å for all three particle types⁴), and the decrease in shell thickness with increasing PPO fraction observed with SANS was not seen with dynamic light scattering. Moreover, the total amount of polymer bound to the particles determined by SANS (shown as the polymer:magnetite mass ratio m_p/m_m in Tables 2 and 3) ranged from 0.45 to 0.54, while thermogravimetric analysis of the particles gave a value of approximately 0.8 for all particles.⁴² A likely reason for these discrepancies in both the shell thickness and the total polymer adsorbed on the particles is that the outer regions of the polymer shell that extend into the solvent phase to provide colloidal stability and that contribute to the hydrodynamic drag on the particles are too dilute to be seen by SANS. The shortfall in polymer content is consistent with an average polymer fraction of approximately 0.015 in this outer shell between L_1 and the hydrodynamic radius. One contributing factor to the large hydrodynamic radius may be that not all the PAA groups are attached to the particle surface and hence the PAA backbone may be able to form loops thereby providing the PEO and PPO side chains greater opportunity to extend even further into the solution than if they were confined to be attached to the particle surface.

A significant trend in the parameters that characterize interparticle interactions is also evident in Tables 2 and 3. For the linear solvation profiles, the value of ζ , the correlation length for particle interactions, was approximately constant for the 12/4 and 8/8 particles at values of 129 and 140 Å, respectively. The 16/0 fit, however,

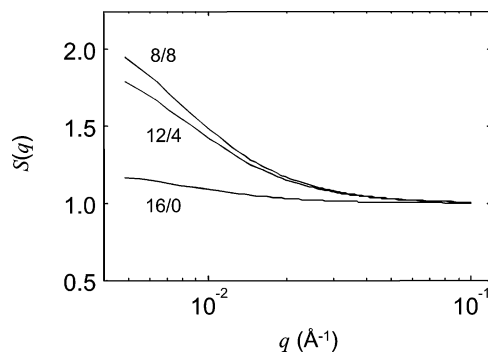


Figure 7. Structure factor for the magnetic fluids as obtained from the fitting procedure. See text. The structure factor increases with increasing PPO content because of attractive interactions.

showed an extremely weak dependence on the structure factor and many pairs of S_0 and ζ values were able to fit the data equally well. To maintain a constant basis of comparison, we fixed the value of ζ for the 16/0 particles at 130 Å—a value consistent with the best-fit value for the other particles. The relatively low value compared to the particle size suggests it probably arises from small particle aggregates. The value of S_0 , related to the osmotic compressibility, increases from 16/0 to 8/8 particles, meaning that adding hydrophobic PPO side chains caused increased interparticle attraction. The magnitude of this attraction is relatively small, however, which is consistent with our observation that the particles do not flocculate. Figure 7 shows the structure factor $S(q)$ calculated using the fitted S_0 and ζ values in Table 2. $S(q) \approx 1$ for the 16/0 particles throughout the entire q range. Attractive interactions for the 16/0 particles are expected to be extremely low as PEO is well solvated and should provide a good steric barrier. In addition, the particle volume fraction was sufficiently low that hard-sphere repulsion should not have played a significant role. A substantial increase in $S(q)$ is observed upon adding PPO side chains, although the actual $S(q)$ remains low compared to that in many other systems. For example, fatty acid-coated aqueous magnetic fluids that showed significant aggregation had a value of $S(q) \approx 600$ at low q .¹⁷ Our decision to fit the core parameters in the range $0.03 < q < 0.1$ Å⁻¹ is validated by Figure 7, which shows that $S(q)$ had diminished to less than 1.08 for all particles by $q = 0.03$ Å⁻¹.

In summary, both models for solvent penetration show a decreasing shell thickness, decreasing solvation, and increasing particle–particle interactions in going from 16/0 to 8/8 particles, i.e., as the PPO fraction in the stabilizing copolymer shell is increased. These effects are all consistent with the exclusion of water from the interior of the shell as the hydrophobicity within the shell increased on addition of these PPO side chains. Although there were some discrepancies between the dimensions from SANS and from other methods, these are most likely a result of our application of a simple model for the particle shape to particles that seem to contain significant shape irregularities. Regardless, neutron scattering does provide experimental insight into the structure within the polymer shell that cannot be easily measured with other techniques.

Mean-Field Lattice Modeling

A mean-field lattice model was used to predict the solvation structure of our magnetic particles by estimating the volume fraction profiles of water, EO, and PO in the

polymer shell. We provide here a short account of the theory adapted to the polymer-coated particles, results of the model calculations, and a comparison between the model predictions and the SANS data. A detailed description of the theory can be found in the literature.^{24,25}

Overview of Theory. In our application, the neighborhood of a particle is divided into concentric layers numbered $i = 1, 2, \dots, M$, starting with the layer next to the spherical core. Each layer is furthermore divided into L_i lattice sites, the number of sites increasing with i . The thickness of the layer corresponds to the size of an EO or a PO monomer. The lattice is completely filled by a mixture of polymer and solvent. The spherical core representing the magnetic particles is considered to be impenetrable to both polymer and solvent. Within each layer, the Bragg–William approximation of random mixing is applied, and hence all lattice sites in a layer are equivalent and the problem becomes essentially one-dimensional.

A key to capturing the complex phase behavior of EO-containing polymers in water is the assumption that PEO exists in a number of conformers owing to trans and gauche bond conformations. The set of conformers could be divided into two classes, one polar and better hydrated and one nonpolar and poorly hydrated.²³ With this approach and a similar one for PO-containing polymers in water,²⁵ binary^{23,25} and ternary²⁶ phase diagrams of PEO, PPO, and water mixtures have been reproduced without the use of temperature- and concentration-dependent parameters.

Our goal in the lattice modeling is to predict the water, EO, and PO volume fraction profiles near the spherical core. These profiles are derived from the canonical partition function, Q , where

$$Q = \Omega \exp(-\beta A_{\text{int}}) \exp(-\beta U) \quad (15)$$

with A_{int} being the internal free energy, Ω the configurational degeneration, U the configurational energy of the system, and $\beta = 1/kT$.

The internal free energy arises from the presence of the internal states, describing the polar–nonpolar equilibrium, and is independent of the polymer configuration of the polymers in the lattice. It is given by

$$\beta A_{\text{int}} = \sum_i \sum_A n_{Ai} \sum_B P_{ABi} [\beta U_{AB} + \ln(P_{ABi}/g_{AB})] \quad (16)$$

where the sums are taken over i (the layers), A (the three components), and B (all states of component A). In eq 16, n_{Ai} is the number of sites in layer i occupied by component A , P_{ABi} is the fraction of component A in layer i that is in state B , U_{AB} is the internal energy of component A in state B , and g_{AB} is the degeneration factor of state B of component A (i.e., the number of B -state conformations of component A).

The configurational degeneration, relative to a reference state, can be expressed as

$$\ln \frac{\Omega}{\Omega^*} = - \sum_A \sum_c n_{Ac} \ln \frac{n_{Ac} r_A}{\omega_{Ac}} \quad (17)$$

where n_{Ac} denotes the number of chains of component A in conformation c , r_A the number of monomers of component A , and where ω_{Ac} is related to the degeneration of component A in conformation c .

The configurational energy is found by adding all nearest neighbor interactions, including surface interactions, and with the mean-field approximation it is given by

$$\beta U = \frac{1}{2} \sum_{i=0}^M L_i \sum_A \sum_{A'} \sum_B \sum_{B'} \phi_{Ai} P_{ABi} \chi_{BB'} \langle P_{A'B'} \phi_{A'i} \rangle \quad (18)$$

where the sums are taken over layer i and component A in state B with another component A' in state B' . Moreover, $\langle \dots \rangle$ represents an average over layers $i - 1$, i , and $i + 1$, including the surface layer ($i = 0$) and ϕ_{Ai} the volume fraction of component A in layer i (our final goal). In eq 17, $\chi_{BB'}$ denotes the interaction parameter between component A in state B and component A' in state B' . It is essentially a Flory–Huggins interaction parameter; however, unlike the standard Flory–Huggins parameter, it needs not to be a function of temperature and/or concentration to accurately reproduce the phase behavior of polymers. Instead the effective interaction between two components becomes temperature and/or concentration dependent from the displacement of the equilibrium between the polar and nonpolar states with temperature and concentration.²⁵

Briefly, the equilibrium condition of the system is characterized by an equilibrium state distribution $\{P_{ABi}\}$ and an equilibrium conformation distribution $\{n_{Ac}\}$. These equilibrium distributions are both implicitly given, and hence they need to be determined self-consistently. Moreover, the two sets are interdependent, and consequently they also need to be determined simultaneously. From the set $\{n_{Ac}\}$, the equilibrium segment distribution $\{n_{Ai}\}$ can be evaluated, and finally the set of volume fraction profiles $\{\phi_{Ai}\}$ is readily available.

Polymer Model. In applying the lattice theory to our polymer-coated particles, we made the simplifying assumption that the polymer shell is composed of PEO and PPO chains that are end-grafted to the cores of the particles. We did not explicitly include PAA in the model, because it is present in a relatively low amount and the geometry of the backbone would complicate the model. To account for the alkyl chain that forms the PAA backbone, the surface of the core was considered to be hydrophobic. We assumed that both the PEO and PPO chains were linear homopolymers of molecular weight 3000 and 2000 g/mol, respectively, which led to $r_{\text{PEO}} = 68$ and $r_{\text{PPO}} = 34$ monomers, respectively. The use of the median magnetite core radius $R_{c,\text{med}} = 36 \text{ \AA}$ and the core polydispersity $\sigma_c = 0.3$ gave a mean core radius $R_c = 37.5 \text{ \AA}$. From (i) the bound polymer–magnetite mass ratio of 0.8, (ii) the total surface area of polydisperse magnetite particles, and (iii) the molecular weight and the ratio of the side chains of the graft copolymer, the grafting densities were determined to 1.17 PEO chains/nm² (16/0 particles), 0.943 PEO and 0.314 PPO chains/nm² (12/4 particles), and 0.682 PEO and 0.682 PPO chains/nm² (8/8 particles). A lattice cell size of 4.0 \AA was then employed to convert from SI units to lattice units. This cell size has been found reasonable in other comparisons involving PEO–PPO–PEO triblock copolymers.^{28,31} Throughout, the temperature was fixed at 300 K.

Interaction Parameters. For our system, 18 independent parameters specifying the internal equilibrium and the interactions need to be specified. These parameters and their values used are collected in Table 4.

Fourteen of the parameters concern the interactions between water, EO, and PO, and they have been determined by extensive regression against PEO–water, PPO–water, and PEO–PPO–water phase diagrams over a range of temperatures. Moreover, they have also been shown to successfully predict the phase behavior of PEO–PPO block copolymers, including the critical micellization temperature and the micelle structure,^{27,30,31} and so they

Table 4.

Parameters Used in Mean-Field Lattice Modeling					
component	state	U_{AB} (kJ/mol)	g_{AB}		
water		0	1		
EO	polar	0	1		
EO	nonpolar	5.086 ^a	8 ^a		
PO	polar	0	1		
PO	nonpolar	11.5 ^a	60 ^a		
$kT\chi_{BB}$ or $kT\chi_{BS}$ (kJ/mol)					
	EO (polar)	EO (nonpolar)	PO (polar)	PO (nonpolar)	surface
water	0.6508 ^a	5.568 ^a	1.7 ^b	8.5 ^b	4.0 ^d
EO(polar)		1.266 ^a	1.8 ^c	3.0 ^c	2.0 ^d
EO(nonpolar)			0.5 ^c	-2.0 ^c	2.0 ^d
PO(polar)				1.4 ^b	0 ^d
PO(nonpolar)					0 ^d

^a From the fit to the experimental data of the binary PEO/water phase diagram (see refs 23 and 24). ^b From the fit to the experimental data of the binary PPO/water phase diagram (see ref 25). ^c From the fit to the experimental data of the ternary PEO/PPO/water phase diagram (see ref 26). ^d Assigned in this work, see text.

should be accurate for the polymer shells of the polymer-coated particles. In more detail, four parameters are related to the internal free energy of the EO and PO segments and dominate the entropy–enthalpy balance of the polar–nonpolar equilibrium. The other 10 parameters, χ_{BB} , describe the state–state interaction among water, EO, and PO.

The remaining four independent parameters involve the interaction with the surface. Of the five surface parameters, only four are independent, and for simplicity $\chi_{POpolar,surface} = 0$ has been adopted. A further simplification was made by assigning $\chi_{EOpolar,surface} = \chi_{EOnonpolar,surface}$ and similarly for PO. The remaining two nonzero values were selected to correspond to a hydrophobic surface representing a PAA layer. Model calculations with all surface interaction parameters equal to zero, referred to as athermal condition, were also performed, and some of these results will also be discussed.

Results of Lattice Modeling. The calculated volume fraction profiles of water, EO, and PO are shown in Figure 8 as a function of distance from the surface for the three types of polymer-coated particles. The layer number has been transformed to distance by multiplying by the lattice size. In Figure 8a, the calculated EO volume fraction profile for the 16/0 particles is approximately linear and decays to zero at ~ 70 Å from the surface. The extension of the chains is consistent with a relatively high grafting density that results in significant repulsion between the chains. The use of an athermal surface reduced slightly the EO volume fraction in the first two layers but had essentially no effect on the EO profile further away from the surface (data not shown). Hence, the predicted linear profile is only marginally influenced by the polymer–surface interactions, making these values not particularly critical for the model results. This fact also implies that it is the solvency of the EO and PO in water that primarily governs the water penetration.

The calculated water, EO, and PO volume fraction profiles for the 12/4 and 8/8 particles are illustrated in parts b and c of Figure 8. A comparison of the profiles shows that increasing the fraction of PPO chains hinders water penetration into the polymer shell. The more hydrophobic character of the PO monomer as compared to EO (cf. Table 4) is responsible for the enhanced polymer

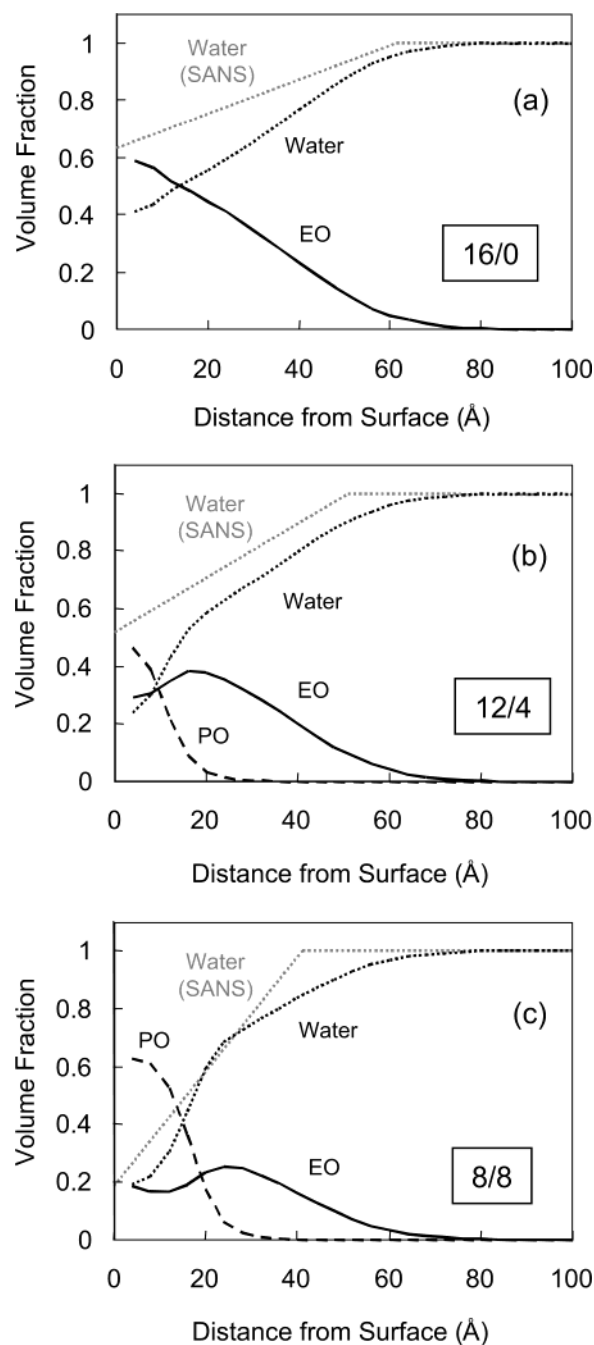


Figure 8. Water, EO, and PO volume fraction profiles in the polymer shell for (a) 16/0, (b) 12/4, and (c) 8/8 particles as predicted from the mean-field lattice modeling and extracted from the SANS data using the linear solvent profile (labeled SANS).

density in the first few layers and the concomitant reduced water penetration. For example, the 8/8 particles have a ~ 15 Å region around the core where the PO volume fraction is larger than 0.40. In this region, the more hydrophilic EO is somewhat excluded, and the EO volume fraction profile shows a slight minimum at ~ 10 Å. This minimum is observed also for the athermal surface condition. The EO–PO repulsion is however not able to establish a full segregation, since the PEO chains are tethered to the core as well. The outer part of the polymer shell contains extensively hydrated EO monomers. Hence, the model predictions support our notion (i) that the polymer shell has an inner region for organic solubilization and (ii) that the particles are stabilized by an extended layer of hydrated EO.

The structure of the polymer shell is qualitatively similar to that of Pluronic micelles composed of PEO–PPO–PEO triblock copolymers. These polymeric micelles have been shown experimentally and theoretically to consist of PPO-rich cores surrounded by a well-solvated PEO corona. Neutron scattering studies have shown that PPO is preferentially located in the core and PEO in the corona of these micelles²⁰ and that a significant amount of water may appear in the PPO-rich core, depending on the particular copolymer and temperature.^{16,20,21} Mean-field lattice modeling provides a similar picture. For example, volume fraction profiles of EO₃₀–PO₆₁–EO₃₀ micelles are similar to that of the polymer shell of the 8/8 particle shown in Figure 8c except that the EO volume fraction was only 0.05 in the first layer of the micelle,³⁰ and similar results are seen for many other types of PEO–PPO–PEO micelles.^{28,30} The lower EO volume fraction in micelles is conceivable, since the PEO chain is not tethered at the center of the micelle. The water volume fraction in the first layer of the polymer shell (0.20) is consistent with the values predicted at the center of Pluronic micelles (0.10–0.35).^{28,30}

Comparison with SANS Results. The predicted water penetration profiles compare reasonably well with those extracted from the best fit to the SANS data using the linear solvent profile, as seen in Figure 8.

Both the measured and the predicted profiles display the largest amount of water near the core for the 16/0 particles and smallest amount for the 8/8 particles, reflecting the anticipated reduction in the water concentration near a particle with increasing PPO fraction. For the 16/0 particles, the water volume fraction at the core surface as predicted from the lattice modeling (0.40) is lower than the corresponding value extracted from the SANS experiments (0.63). Figure 8b demonstrates that the same holds also for the 12/4 particles, but Figure 8c displays a smaller difference for the 8/8 particles.

The functional form of the water penetration profile predicted by the model supports the linear water profile for the 16/0 particles assumed in the analysis of the experimental SANS data. With increasing PPO fraction, however, the predicted water profile becomes increasingly nonlinear and can be described well as having two linear regimes with a larger slope for the inner layer. However, a refitting to the SANS data using two continuous linear regions did not improve the fit. More complex functional forms such as an exponential decay function²¹ or Fermi–Dirac distribution function⁴¹ have been applied to model solvent penetration, but these have no explicit analytical form for the scattering and have typically been applied to much more monodisperse micellar systems.

The extension of the polymer shells is qualitatively the same for the profiles extracted from the SANS data (~40–60 Å) and from the model predictions (~60 Å), with the one difference that the thickness of the polymer layer extracted from the SANS data is reduced as the PPO fraction is increased while the model predicts no effect of PPO on this extension. This discrepancy may be due to an effective averaging of the slopes by the SANS fitting routine or to the differences in the particle sizes measured using TEM (used in the lattice calculations) and those extracted during the SANS analysis. In neither case is the polymer shell thickness as large as that determined by dynamic light scattering, whose technique is sensitive to irregularly shaped particles and is sensitive to polymer chains extending further out into the solution; such extensions may be possible because experimentally the PAA may not all be confined to the particle surface and may extend into the polymer shell, permitting the attached

PEO and PPO chains to extend even further into the solution than if they were attached directly to the particle surface as has been assumed in the modeling. These dangling chains would have a significant effect on the hydrodynamic diameters of the particles but may be too dilute in solution to be observed by SANS.

We note that neither the SANS experiments nor the lattice model is capable of predicting angular inhomogeneity in the shell, as the SANS models were centrosymmetric and the lattice model assumed random mixing within a layer.

Conclusions

The hydration structure of the polymer shells of a class of PEO/PPO polymer-stabilized magnetic nanoparticles has been examined both experimentally, with small-angle neutron scattering, and theoretically, using a mean-field lattice model. The hydration structure is important because these polymer shells have been designed to provide an inner hydrophobic region for the extraction of organic compounds and an outer hydrophilic region to provide steric stabilization in water.

SANS experiments with our magnetic fluids showed that when the particles were suspended in H₂O-rich solvents, the scattering was primarily from the magnetite core, while in D₂O-rich solvents the scattering was primarily from the polymer shell. From these data, we extracted the sizes of the magnetic cores, which were found to be significantly different from those measured by TEM; the differences were attributed to the irregular shapes of the particle cores. The shell hydration and interparticle interaction parameters were determined via a global fit of the scattering data in five H₂O/D₂O mixtures of varying levels of deuteration to provide contrast variations. We successfully fit the scattering data with a core–shell model for the particles with both a linear and a constant solvent profile in the shell. With both models, we observed a significant trend in the shell hydration, in that replacing PEO side chains with PPO side chains led to a contraction of the polymer shell and exclusion of water near the magnetite surface. In addition, from the interparticle structure factor a slight attraction between particles was inferred to appear.

Mean-field lattice modeling of end-grafted polymer chains provided another method of determining the structure in the polymer shell. This technique was able to predict both the water penetration profile and the distribution of EO and PO monomers in the shell. This latter information could not be determined with neutron scattering without deuterating either the PEO or PPO chains due to their similar scattering length density. The predicted hydration profiles were qualitatively similar to those determined by neutron scattering, in that the replacement of PEO chains with PPO chains led to the formation of a water-excluded zone near the particle surface. The water density near the particle core is similar to that seen in the cores of Pluronic micelles. The modeling showed that the shorter and more hydrophobic PPO chains were concentrated near the magnetite surface while PEO chains extended away from the surface. There was some evidence of PEO exclusion from the PPO-rich region, although less than is typically observed in modeling of structurally similar Pluronic micelles due to the chemical attachment of the PEO chains to the surface of the magnetite particles. As in Pluronic micelles, the transition between the PPO-dominated and PEO-dominated regions is diffuse and the hypothesized structure in Figure 1 is therefore highly idealized.

Finally, our nanoparticles⁴ are known to solubilize significant quantities of hydrophobic organics in water like the Pluronic micelles do. However, we note that the nanoparticles offer several advantages over the micellar systems for separation, as they retain their PPO domain structure when diluted and have the potential to be recovered by magnetic filtration.

Acknowledgment. This work was supported by the National Science Foundation (CTS-9817221) and the Singapore–MIT Alliance (SMA). G. Moeser would like to thank the Eastman Kodak Company for support with a

Kodak Fellowship. We thank Mike Frongillo (MIT, CSME) for his assistance with the TEM measurements and Steve Kline (National Institute of Standards and Technology) for his assistance with the planning and execution of the SANS experiments. We acknowledge the support of the National Institute of Standards and Technology, U.S. Department of Commerce, in providing the neutron research facilities used in this work. This work utilized facilities supported in part by the National Science Foundation under Agreement No. DMR-9986442.

LA036240K